AN INVESTIGATION OF THE FINE RAY STRUCTURE OF THE CORONAL STREAMER BELT USING LASCO DATA

V. G. ESELEVICH and M. V. ESELEVICH
Institute of Solar-Terrestrial Physics, Irkutsk, Russia (E-mail: esel@iszf.irk.ru)

(Received 26 January 1999; accepted 3 May 1999)

Abstract. It is shown that within $R > 3–4\ R_\odot$ from the solar center the coronal streamer belt consists in a sequence of radial brightness rays. A minimum angular size of the individual ray $d \approx 2.0° – 2.5°$, which is about the same in the directions normal to and along the streamer-belt, is independent of the distance from the Sun at $R = 4–6\ R_\odot$. The lifetime of the rays can exceed 10 days. From time to time, inhomogeneities of material inside the rays begin to move in the antisunward direction. Plots of increase in their velocity with the distance from the Sun are similar to those obtained by Sheeley *et al.* (1997) for inhomogeneities that are carried by a quasi-stationary solar wind in streamers. It is concluded that the phenomena discussed in this paper and by Sheeley *et al.* (1997) share a common origin. It is suggested that a different origin of solar wind flows in streamers and in coronal holes may be associated with a different character of flows in microtubes of the magnetic field comprising a total solar wind flow. These tubes are observed as brightness rays in streamer belts and plumes in coronal holes.

1. Introduction

The existence of the coronal streamer belt which separates regions in the corona with the radial magnetic field of the Sun of opposite polarity is well documented in many publications (See, e.g., Svalgaard, Wilcox, and Duvall, 1978; Korzhov, 1977; Gosling *et al.*, 1981) and is confirmed by coronal magnetic field calculations in a potential-field approximation (Burlaga, Hundhausen, and Zhao, 1981; Wilcox and Hundhausen, 1983). A neutral line of the radial magnetic field runs along the belt. In heliospheric space, such a belt represents a 'skirt' of increased density and pressure curving around the Sun which is called the heliospheric plasma sheet (Crooker *et al.*, 1993). A slow solar wind of increased density flows in its neighbourhood with velocity as high as 300–400 km s^{-1} at 1 AU (Borrini *et al.*, 1981; Feldman *et al.*, 1981; Gosling *et al.*, 1981). The base of the streamer belt on the Sun is the site of initiation of coronal mass ejections (CME) (Hundhausen, 1993; Mendoza and Perez-Enriquez, 1993; Eselevich, 1995; Eselevich and Tong, 1997), and the heliospheric plasma sheet has a pronounced effect on the formation and propagation of shock waves (Eselevich, Fainshtein, and Filippov, 1988; Eselevich, 1990). The streamer belt evolves relatively slowly over a solar activity cycle. The characteristic time of this evolution for minimum solar activity is comparable with the period of a Carrington rotation. During periods of increased solar activity, the

Solar Physics **188:** 299–313, 1999.

streamer structures, under the influence of CMEs, can undergo faster changes with a typical time of about 24 hours (Illing and Hundhausen, 1986). At quiet times (i.e., in the absence of CMEs), MacQueen and Poland (1977) and Poland (1978) reported also nearly twofold changes in brightness of the streamer belt between its two recordings on the limb (at intervals of 24 hours or shorter). According to Crooker *et al.* (1993), such changes in brightness can be caused by an instability of the streamer belt. However, an alternative explanation is also possible: these changes can be a manifestation of the spatial inhomogeneity of the brightness distribution along the belt. To distinguish between spatial and temporal changes in brightness along the streamer belt, Eselevich (1998) investigated the part of the streamer belt which follows a meridian of longitude near the west or east limb. In this case the limb plane will show a virtually instantaneous picture of the brightness distribution along that part of the belt, thus minimizing the effect of any time variation. It was shown that the brightness distribution along the streamer belt is nonuniform, and within distances more than three solar radii from the solar center they represent a sequence of rays with increased brightness. In the absence of coronal mass ejections, the distribution along the streamer belt with a typical scale of several tens of degrees can remain stable during nearly two complete Carrington rotations (Eselevich, 1998). However, this does not preclude the existence, along the streamer belt, of even smaller-scale and relatively rapidly time-varying structures (with, for example, a typical time of about one hour). Recent measurements acquired by the LASCO instrument showed the existence of small-scale (with the size of several degrees) ray structures in the streamer belt (Wang *et al.*, 1997). Relatively fast changes in brightness (with a typical time of about one hour) caused by radially moving inhomogeneities of material with an initial transverse size of about 0.1 $R_\odot$ were also recorded in streamers (Sheeley *et al.*, 1997). The fine ray structures and their relation to the outward-moving 'blobs' were discussed by Wang *et al.* (1998a). In this paper, it was suggested that the rays are newly reconnected, open magnetic field lines carrying material that was originally trapped inside the closed helmet streamers, and that the blobs are small density inhomogeneities along these rays. Filamentary structures in streamers have also been detected using radio scintillation measurements (Woo *et al.*, 1995).

Taken together these observations suggest that ascertaining the origin of flows in streamers must focus on the study of relatively small-scale and relatively fast varying structures of the belt. The objective of this paper is to investigate the fine (with the scale of about 1 deg) structure of the streamer belt and its possible time variations (at a scale of about 1 hour) using the LASCO C2 and C3 data.

2. Data and Methods of Analysis

2.1. THE DATA ANALYZED

This study is based on the white-light corona brightness data primarily from the LASCO C2 instrument on-board the SOHO spacecraft, as well as from LASCO C3 available in the INTERNET. The C2 and C3 coronagraphs provide white-light corona images within 1.5–6 $R_\odot$ and 3.7–30 $R_\odot$, respectively (Brueckner *et al.*, 1995). Daily images represented in the MPEG format were used. The time between adjacent frames, on average, did not exceed one hour. The data for July–August and also for September 1996, were selectively used in the analysis. The data in the MPEG format are not calibrated but we can say with certainty (and this is confirmed by results of this paper) that these data contain a wealth of unique information about processes in the corona and that if it is used reasonably carefully, one can obtain new important knowledge of the physics of these processes. To minimize the possible influence of the character of the data used in the analysis, we used the following approaches:

(1) We used only sufficiently bright ray structures (whose brightness exceeded markedly the background brightness) within $R = 4$–15 $R_\odot$ from the solar center.

(2) Not absolute brightness distributions of the corona but their relative changes with time were studied. Also, the time interval in each case under investigation did not exceed several days. Therefore, it was possible to exclude the influence of possible gradual changes in instrument characteristics with time.

(3) We studied the radial structures in the corona, the projection Λ of the latitude onto the sky plane of which did not exceed $\pm 30°$. The sign of Λ is positive northward of the equator and negative southward.

2.2. DETERMINING THE RAY BRIGHTNESS P_R, THE ANGULAR SIZE OF RAYS ALONG (d_L) AND NORMAL TO (d_T) THE STREAMER BELT

For each image obtained from daily MPEG files, brightness distributions P of the corona were constructed depending on the angle Λ at different distances R from the solar center, separately for the E and W limbs. A typical form of a portion of such a distribution on E limb in the case when the streamer belt is normal to the sky plane and when the belt is elongated along the limb is shown in Figures 1 and 2, respectively. The profile in Figure 1 clearly shows one brightness maximum (ray), and Figure 2 shows several rays. For investigating the properties of the rays, we introduce the following characteristics: the ray brightness P_R, the angular size of the ray d_T in a direction normal to the streamer belt, and the angular size d_L along the streamer belt. The ray is distinguished on the brightness profile P by the slope of two lines forming it, which from the top to the points A and B may be represented by straight lines. This permits us to introduce the definition of the ray brightness P_R and the angular sizes d_T and d_L as shown in Figures 1 and 2 (top). To unify the process of identifying the ray at the background of the remaining part

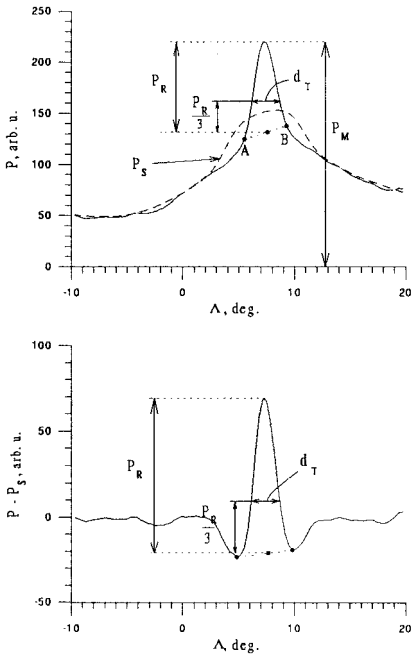

Figure 1. Typical distribution profiles from the angle Λ in the case when the portion of the streamer belt under consideration is normal to the sky plane. *Top*: ray brightness P_R where the smoothing curve P_S is obtained by averaging the curve P over the range of angles of 6–7 deg (dashes in the upper panel). LASCO C2 data for 30 July 1996, 08:05 UT, E limb, $R = 4.5\ R_\odot$.

of the signal and, accordingly, the determination of the ray brightness P_R and of the angular sizes d_T and d_L, the following procedure was used: for each profile, we determined a smoothed curve by averaging over the angle of 6–7 (dashed curve P_S in Figures 1 and 2). After that, this averaged curve was subtracted from the original profile. The result of this procedure is shown in Figures 1 and 2 (bottom). Amplitude values of the ray P_R measured from the schematic representations corresponding to Figures 1 and 2 (top), do not differ by more than 10% for the cases with d_T and $d_L < 3$–4 deg at $R = 3$–$6\ R_\odot$.

3. Analysis of the Structure of the Streamer Belt with High Spatial and Temporal Resolution

3.1. The Angular Size and Radiality of Rays

The angular size and radiality of rays of prime interest is in the region on the synoptic map which includes the area where the neutral line is elongated along the meridian. For CR 1912 (see Figure 3), the longitude range 240–300 deg (or the dates of the central meridian 31 July–6 August 1996) approximately correspond to

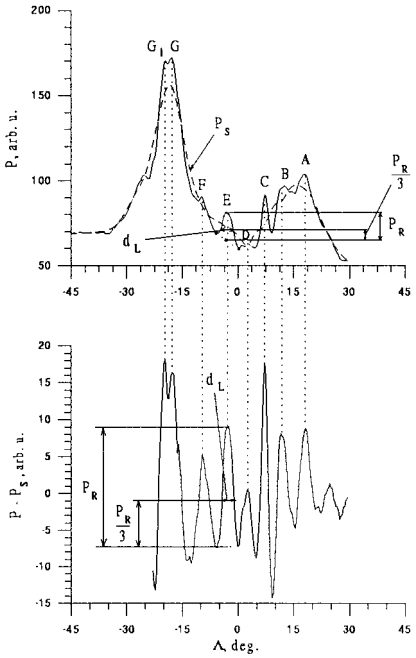

Figure 2. Typical distribution profiles from the angle Λ but in the case when the portion of the streamer belt under consideration is elongated along the meridian. *Top*: brightness P of the white-light corona streamers. *Bottom*: ray brightness P_R; LASCO C2 data for 26 July 1996, 15:49 UT, E limb, $R = 4.5\ R_\odot$.

it. The profile shown in Figure 2 (*bottom*) was obtained at 4.5 $R_\odot$ on the E limb on 26 July 1996 (15:49) and represents a number of rays of different intensities: the rays A, B, C, D, E, F, and G (has two peaks). A minimum angular size $d_L \approx 2.0$–$2.5°$ (ray C). The smallest value of d_T also was ≈ 2.0–$2.5°$ and was measured for the portions of the belt that were parallel to the equator and were of a reasonably large length. For example, such a case occurs on the E limb on 30 July 1996 (08:05 UT) (Figure 1, top). On the synoptic map (Figure 3), it is the portion of the belt with longitude < 225 deg. With an increase in the slope of the streamer belt to the equator, obviously the measured angular size d_T must also increase. It is significant that a minimum angular size of the individual ray is about the same in the directions normal to and along the streamer belt. The radiality of the rays A–F was investigated using the data from the LASCO C2 and C3 instrument. Results are presented in Figure 4 (the rays G and G_1 are closely spaced and were, therefore, excluded from consideration). The figure shows that all rays are aligned along the radius within 4–15 $R_\odot$ with an accuracy not worse than $\pm 1.5°$. Because of its small amplitude, the ray F was recorded to within 6.5 $R_\odot$ only. The angular size of the rays remains almost unchanged within 4–6 $R_\odot$.

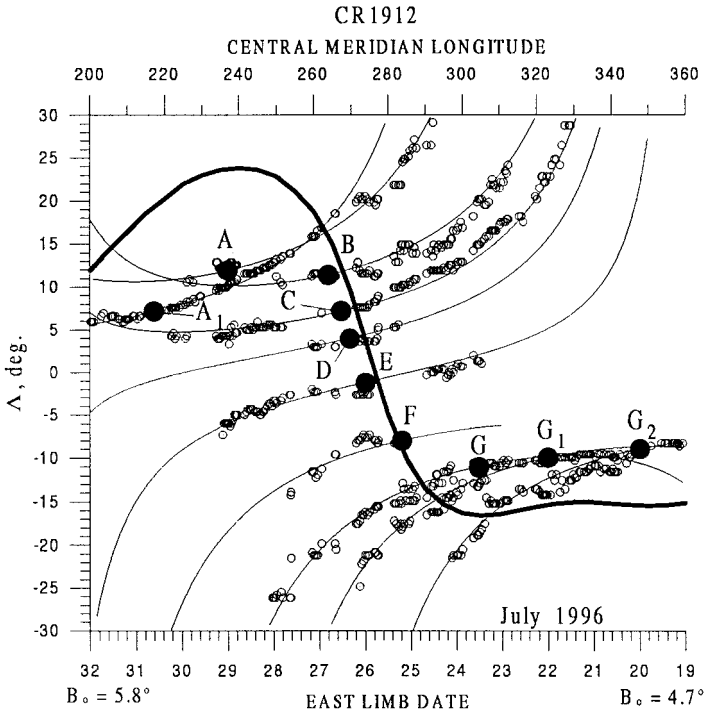

Figure 3. A portion of the synoptic map for CR 19l2. Open circles: experimental variations of the angle Λ for rays recorded on the E-limb, at consecutive instants of time. Large dark circles: anticipated positions of individual brightness rays at the time when they traverse the E-limb. Thin solid lines: calculated variations of the angle Λ for rays marked by dark circles. Thick solid line: neutral line of the mean solar magnetic field constructed according to J. T. Hoeksema's calculation.

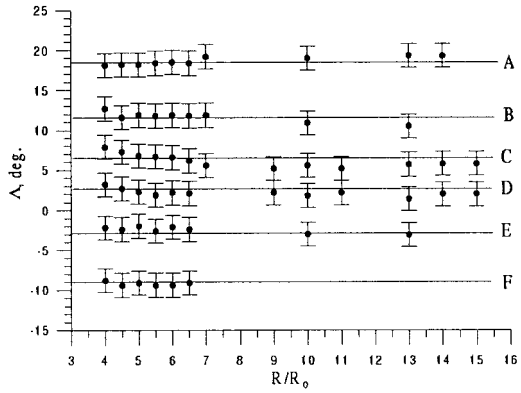

Figure 4. Dependences of Λ on the distance to the solar center for the rays A, B, C, D, E, and F; 26 July 1996, 15:49 UT, E limb.

3.2. TIME VARIATIONS OF THE RAYS

The above data suggest that the streamer belt from 4 $R_\odot$ to 6 $R_\odot$ at a minimum consists of a sequence of relatively narrow radial rays with $d_T \approx d_L \approx 2°–4°$. When the belt is approximately parallel to the solar equator, they merge into a single ray on the limb. When, however, the belt bends, they become more pronounced on the limb with the increasing slope of the belt to the solar equator. Let us try to visualize how the observed picture on the limb will change with the time and, at the same time, to confirm the anticipated belt structure. Let a narrow (in the direction of rotation) ray co-rotating with the Sun traverse the limb plane. In limb measurements, because of the character of the Thompson scattering of photospheric emission from electrons in the corona, the observed brightness of a narrow ray will decrease by a factor of two as one recedes from the plane of sky by $\approx 35°$ (Hundhausen, 1993). The projection of its latitude Λ onto the sky plane will be changing with time, and the character of this variation depends on the ray latitude λ on the Sun and on the heliographic latitude of the solar disk center B_0. Therefore, on the synoptic map the ray will describe a certain curve (see Appendix). Open circles in Figure 3 show experimental positions of the rays on the brightness profile, similar to that shown in Figure 2 (bottom), at consecutive instants of time (the profiles were constructed for the distance 4.5 $R_\odot$ from the solar center).

Solid thin lines show theoretical curves obtained for rays whose positions on the synoptic map at the time when they pass across the limb plane are marked by dark circles. It is evident that the calculated and experimental curves are in reasonably good agreement. Furthermore, the following features should be pointed out:

(1) The rays C, D, E, and F are in isolation because no other rays (or other structures with increased brightness) exist along the parallel at distances >35 degrees on both sides of each of them. The brightest of them, the ray C is recorded with confidence during nearly ± 5 days with respect to the time when it traverses the sky plane, and the rays D, E and F of lower brightness are recorded during 2–5 days. The typical angular distance between each of the adjacent rays C, D, E, and F is $L \approx 4°–7°$ and is comparable with or larger than the angular size d_L of the rays themselves. The mean angular distance between open circles along the curves C–F in Figure 3 is much smaller than the distance L between rays along the belt. This permitted a reliable identification of each of the rays when moving along these curves.

(2) In the northern and southern parts of the belt, respectively, the rays A and A_1, and the rays G, G_1, and G_2 are distinguished, which gradually merge into the streamer belt elongated along the equator. Note that between each pair of these rays one or two rays of a smaller amplitude can be located, and the latitudinal location of their maxima is difficult to ascertain.

(3) The heavy line in Figure 3 shows a neutral line plotted from J. T. Hoeksema's data. One can see that the neutral line position and the calculated position of the rays in the transition region are in good agreement. Agreement between

the profiles of the northern and southern parts of the belt and the neutral line is considerably poorer. This seems to be a consequence of the limited accuracy of calculating the coronal magnetic field in a potential-field approximation. Hence the assumption that the streamer belt consists of rays correlates well with the observed picture on the limb. Also, the lifetime of the rays can exceed 10 days.

An additional study was made of how the brightness P_R of the isolated ray C was changing with time, i.e., along the position of open circles of the ray C in Figure 3. The experimental profile is shown in Figure 5 (top). The solid thick line in this figure shows the theoretical curve (see the Appendix) calculated for the narrow ray located at the point shown in Figure 3 by a dark circle with the index C. One can see that the curves are generally similar in their form, but the experimental profile shows relatively short-duration, random enhancements and decreases of P_R. These time variations in brightness are one of the reasons why it is impossible to trace the latitudinal location of the weakest (in brightness) rays over a reasonably long time interval (rays D, E, and F in Figure 3). Particularly conspicuous in Figure 5 are the fronts of a rapid increase in brightness, with typical times of several hours by the end of 22 July and on 24–25 July. The origin of these fronts can be understood by comparing the P_R profiles of this ray obtained at different radii. Figure 5 (bottom) shows the front of 22 July at 4 $R_\odot$ and 5.5 $R_\odot$. Crosses in the figure mark the middles of the fronts at the half-height. For the lower curve, the definition of the time width of the front Δt is given. The time shift between the middles of the fronts at different R is 3.84 h, which gives the mean velocity within 4.0–5.5 $R_\odot$ $V \approx 76$ km s^{-1}. On estimating the front width at 5.5 $R_\odot$, we have $\Delta \approx \Delta t V \approx 4.8$ $R_\odot$. Similarly, for the second front on 24–25 July we get $V \approx 75$ km s^{-1} and $\Delta \approx 4.0$ $R_\odot$. Thus, fast (with a time scale of several hours) changes in brightness in the isolated ray reflect the antisunward propagation of plasma density inhomogeneities inside the ray. More detailed investigations showed that the velocities of the inhomogeneities increase progressively with distance from the Sun. For the front of 22 July, for example, V increases from $\approx$50 km s^{-1} at 4.0 $R_\odot$ to $\approx$100 km s^{-1} at 6.0 $R_\odot$. Antisunward traveling inhomogeneities with different amplitudes, velocities and widths of the front were recorded inside all rays shown in Figure 3. To all appearances, they occur relatively frequently (about 1–2 events during 1–2 days) and independently in each of the rays. For the isolated rays C, D, E, and F, because of their relatively low contrast, it is rather difficult to measure the dependence to R within distances $\geq$10 $R_\odot$. But this is possible for rays such as A or G in Figure 3 located at points of a maximum deviation of the streamer belt from the equator whose contrast with respect to ambient plasma is several times. Equally well visible, Figure 6 (top) shows the dependence of brightness $P_M(t)$ at $R = 6.0$ $R_\odot$ for such a type of ray that traverses the E limb at the beginning of 22 September 1996 at the latitude $\Lambda \approx 24°$ (CR 1914). One can distinguish fronts of a rapid increase in brightness at the beginning of 20 September (front I) and at the beginning of 21 September (front II). $P_M(t)$-plots obtained for different distances R were used to calculate by the above

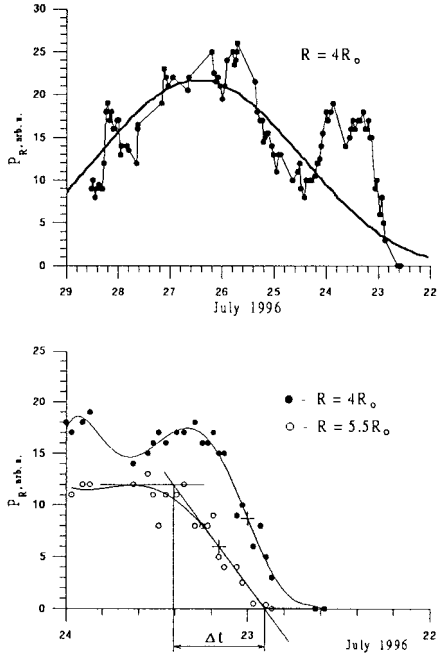

Figure 5. Top: time dependence of the brightness P_R of the ray C, E-limb, $R = 4\ R_\odot$. *Bottom*: a portion of a fast increase of the same dependence $P_R(t)$ of the ray C at $R = 4\ R_\odot$ (dark circles) and $R = 5.5\ R_\odot$ (open circles).

method the velocities V at different distances and to construct the dependencies $V(R/R_\odot)$ of the propagation of these fronts inside the ray (Figure 6, bottom). The initial segments of these curves are characterized by accelerations of $\approx$5 m s^{-2} and 8 m s^{-2}, respectively. Solid curves show the approximation of experimental points by the function (Sheeley *et al.*, 1997): $V^2 = V_0\,(1 - \exp(-(r - r_1)/r_a))$ where for front I: $r_a = 3.0\ R_\odot$; $V_0 = 172$ km s^{-1}, $r_1 = 4.9\ R_\odot$; and for front II: $r_a = 4.0\ R_\odot$; $V_0 = 330$ km s^{-1}, $r_1 = 4.9\ R_\odot$.

The dependencies in Figure 6 are similar to the $V(R)$-plots in Figures 5 and 8 from Sheeley *et al.* (1997) obtained for radially traveling inhomogeneities in streamers. It is significant that Sheeley *et al.* and we used different techniques for measuring $V(R)$. According to Sheeley *et al.*, inhomogeneities move further away from the Sun with initial angular size of 0.1 $R_\odot$ comparable with the ray's angular size. Therefore, it is safe to assume that in both their and our case we are concerned with the same phenomenon: inhomogeneities of material traveling inside the ray in the antisunward direction. According to the conclusions drawn by Sheeley *et al.* (1997), the inhomogeneities are carried by a quasi-stationary solar wind flowing along the rays. We wish to note without questioning this conclusion that the velocity of the inhomogeneity with respect to the solar wind in individual rays can be comparable with or larger than the velocity of the solar wind itself. Indeed, if it is assumed that for front I in Figure 6, $V \approx 170$ km s^{-1} is the velocity

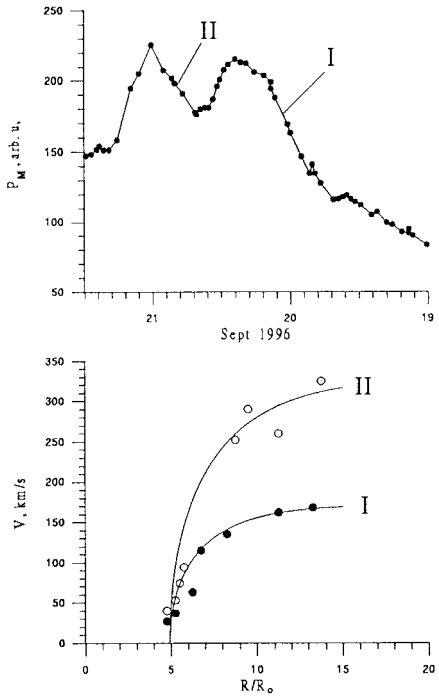

Figure 6. Top: time dependence of maximum brightness P_M for the ray that traverses the E-limb at the beginning of 22 September 1996 at the latitude $\Lambda = 24°$ (CR 1914), $R = 6\ R_\odot$. *Bottom*: dependencies on the distance R from the Sun along the ray under considerations of the velocity of brightness growth fronts I (dark circles) and II (open circles).

with which the inhomogeneity is carried by the solar wind flowing in the ray, then front II propagates with respect to this wind with $V \approx 150$ km s^{-1}.

4. Discussion of Results

The analysis made in this paper has shown that the streamer belt is a sequence of radial brightness rays whose angular size remains unchanged outward from the Sun within distances $R > 4{-}6\ R_\odot$. Preliminary investigations based on the LASCO C1 data suggest that within distances $1.1\ R_\odot < R < 3\ R_\odot$ the angular size of these rays also remains invariable and is $\approx 2{-}3°$, and as the solar surface is approached the rays themselves are gradually deflected from their radial direction by an angle of $\approx 10{-}20°$, bending around the helmet. Since the plasma in the corona is characterized by high conductivity, the observed brightness distribution inside each ray, and also a different brightness behaviour with the time in neighbouring rays testifies that each ray is isolated from neighbouring rays, and this isolation can be ensured by the magnetic field only. Hence, the rays constitute magnetic flux tubes. Note that plumes forming a flow in coronal holes also represent magnetic

tubes with the diameter at the base approximately equal to 2.0–2.5 deg or the supergranule size. However, unlike magnetic tubes within the streamer belt, these plumes undergo a superradial divergence (Thieme, Marsch, and Schwenn, 1987; DeForest *et al.*, 1997), and their typical angular size varies from 2.5° at 1.05 $R_\odot$ to 7° at 5 $R_\odot$, and to ≈15° at 15 $R_\odot$ from the solar center (DeForest *et al.*, 1997), i.e., it can be nearly six times greater than the angular size of a supergranule. Movements of inhomogeneities (so-called jets) were also recorded in plumes, but with higher velocities than in streamers (as high as 1000 km s^{-1}) (Wang *et al.*, 1998b). It is quite possible that the origin of flows both in streamer belts and in the coronal hole is determined by the character of flows in magnetic tubes which constitute these flows.

5. Conclusions

(1) It has been shown that within distances $R > 3–4\ R_\odot$ from the solar center the streamer belt represents a sequence of radial rays of brightness. A minimum angular size of a single ray $d \approx 2.0°–2.5°$ is about the same in the directions normal to and along the streamer belt and is independent of the distance from the Sun at $R = 4–6\ R_\odot$. The lifetime of the rays can exceed 10 days.

(2) It has been shown that antisunward traveling inhomogeneities of material are produced inside the rays intermittently. Plots of increases in their velocities with the distance from the Sun are similar to those reported by Sheeley *et al.* (1997) for inhomogeneities carried by a quasi-stationary solar wind in streamers. It is concluded that the phenomena investigated is this paper and in a paper of Sheeley *et al.* share a common origin.

(3) It has been suggested that a different origin of solar wind flows in streamers and in coronal holes can be associated with a different character of flows in microtubes of the magnetic field comprising a total solar wind flow. These tubes are observed as rays of brightness in streamer belts and as plumes in coronal holes.

Appendix

Hundhausen (1993) reported a dependence of the projection onto the sky plane of the latitude Λ of a radial narrow ray originating from the solar surface on its actual latitude λ on the solar surface and on the longitude ψ_L measured from the solar limb. In the expression for Λ, we take into account the dependence on the heliographic latitude B_0 (Figure 7). Let $x'y'z'$ be a cordinate system tied to the Sun in such a manner that the solar equator lies in the plane $x'y'$ and the Earth the plane $x'z'$. It is obvious that

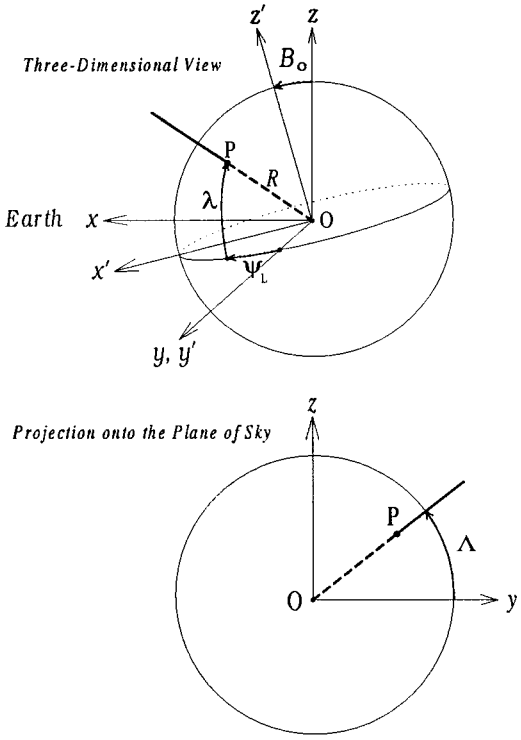

Figure 7. Schematic representation illustrating the determination of the angle Λ.

$$x' = R\cos\lambda\sin\psi_L\ ,$$
$$y' = R\cos\lambda\cos\psi_L\ , \tag{1}$$
$$z' = R\sin\lambda\ .$$

Going to the coordinate system xyz tied to the observer is ensured by a rotation by the angle B_0 about the axis y':

$$x' = -z\sin B_0 + x\cos B_0\ ,$$
$$y' = y\ , \tag{2}$$
$$z' = z\cos B_0 + x\sin B_0\ .$$

By equating (1) and (2), we obtain:

$$\begin{aligned} x\cos B_0 - z\sin B_0 &= R\cos\lambda\sin\psi_L\ ,\\ x\sin B_0 + z\cos B_0 &= R\sin\lambda\ , \qquad (3)\\ y &= R\cos\lambda\cos\psi_L\ . \end{aligned}$$

We now write the expressions for x and z:

$$\tan\Lambda = z/y,\ z = y\tan\Lambda = R\cos\lambda\cos\psi_L\tan\Lambda\ ,$$

$$x = \sqrt{R^2 - y^2 - z^2} = R\sqrt{1 - \cos^2\psi_L(1+\tan^2\Lambda)} = \\ = R\sqrt{1 - \frac{\cos^2\lambda\cos^2\psi_L}{\cos^2\Lambda}}\ ,$$

and substitute them into the first two equations of the system (3):

$$R\cos B_0\sqrt{1 - \frac{\cos^2\lambda\cos^2\psi_L}{\cos^2\Lambda}} - \\ -R\cos\lambda\cos\psi_L\tan\Lambda\sin B0 = R\cos\lambda\sin\psi_L\ ,$$

$$R\sin B_0\sqrt{1 - \frac{\cos^2\lambda\ \cos^2\psi_L}{\cos^2\ \Lambda}} + R\ \cos\ \lambda\ \cos\ \psi_L\ \tan\ \Lambda\ \cos\ B_0 = R\ \sin\ \lambda\ .$$

By multiplying the first equation by $\cos B_0$ and the second by $\sin B_0$ and adding them together, we get

$$\sqrt{1 - \frac{\cos^2\ \lambda\ \cos^2\psi_L}{\cos^2\ \Lambda}} = \cos\ \lambda\ \cos\ B_0\ \sin\ \psi_L + \sin\ \psi_L + \sin\ B_0\ , \tag{4}$$

or

$$\cos\ \Lambda = \frac{\cos\ \lambda\ \cos\ \psi_L}{\sqrt{1 - (\cos\ \lambda\ \cos\ B_0\ \sin\ \psi_L + \sin\ \lambda\ \sin\ B_0)^2}}\ . \tag{5}$$

Expression (5) gives the desired dependence for Λ on λ, ψ_L and B_0. When $B_0 = 0$ it coincides with that reported by Hundhausen (1993). As pointed out by Hundhausen, the scattering function of photospheric emission from a narrow radial ray of increased density that traverses the plane of sky as a consequence of solar rotation at a given heliocentric distance $R > 2\ R_\odot$ (limb darkening may be neglected) in the case of spherical symmetry and the power law $n \approx r^{-5}$ of density decrease in the corona has the form:

$$i(\theta) \approx \left(\frac{R}{R_\odot}\right)^2 [2C - A\ \cos^2\ \theta]\ \cos^3\ \theta\ , \tag{6}$$

where

$$A = \left(\frac{R_\odot}{R}\right)^2 \left[1 - \left(\frac{R_\odot\ \cos\ \theta}{R}\right)^2\right]^{1/2}\ \cos^2\ \theta\ ,$$

$$C = \frac{4}{3} - \left[1 - \left(\frac{R_\odot\ \cos\ \theta}{R}\right)^2\right]^{1/2} - \frac{1}{3}\left(\frac{R_\odot\ \cos^2\ \theta}{R}\right)^{3/2}\ ,$$

where θ is the angle of deviation of the ray along the line of sight from the plane of sky. In view of (4), the dependence of θ on B_0 and λ is represented as:

$$\sin\,\theta = \frac{x}{R} = \cos\,\lambda\,\cos\,B_0\,\sin\,\psi_L + \sin\,\lambda\,\sin\,B_0\,. \tag{7}$$

Acknowledgements

The SOHO/LASCO data used here are produced by a consortium of the Naval Research Laboratory (USA), Max-Planck-Institute für Aeronomie (Germany), Laboratoire d'Astronomie (France), and the University of Birmingham (UK). SOHO is a project of international cooperation between ESA and NASA. Wilcox Solar Observatory data was obtained via web site http://quake.stanford.edu/wso at 1998:05:14 –18:43:35 PDT courtesy of J. T. Hoeksema. The Wilcox Solar Observatory is supported by NASA, NSF, and ONR. We are grateful to S. M. Churilov for useful discussions and to V. G. Mikhalkovsky for his assistance in preparing the English version of the manuscript. This work was partially supported by a Grant from the Russian Foundation for Fundamental Research and Chinese Foundation of Science Research (Grant N960200002c). Grant governmental support for Russian Federation's leading scientific schools N961596733 and GNTP 'Astronomy'.

References

Borrini, G., Wilcox, J. M., Gosling, J. T., Bame, S. J., and Feldman, W. C.: 1981, *J. Geophys. Res.* **86**, 4565.
Brueckner, G. E. *et al.*: 1995, *Solar Phys.* **162**, 357.
Burlaga, L. F., Hundhausen, A. J., and Zhao, X.: 1981, *J. Geophys. Res.* **86**, 8893.
Crooker, N. U., Siscoe, G. L., Shodhan, S., Webb, D. F., Gosling, J. T., and Smith, E. J.: 1993, *J. Geophys. Res.* **98**, 9371.
DeForest, C. E. *et al.*: 1997, *Solar Phys.* **175**, 393.
Eselevich, V. G.: 1990, *Planetary Space Sci.* **38**, 189.
Eselevich, V. G.: 1995, *Geophys. Res. Letters* **22**(20), 2681.
Eselevich, V. G.: 1998, *J. Geophys. Res.* **103**, 2021.
Eselevich, V. G. and Fainshtein, V. G.: 1992, *Planetary Space Sci.* **40**, 105.
Eselevich, V. G. and Tong, Y.: 1997, *J. Geophys. Res.* **102**, 4681.
Eselevich, V. G., Fainshtein, V. G., and Filippov, M. A.: 1988, *Planetary Space Sci.* **35**, 1015.
Feldman, W. C., Asbridge, J. R., Bame, S. J., Feinmore, E. E., and Gosling, J. T.: 1981, *J. Geophys. Res.* **86**, 5408.
Gosling, J. T., Borrini, G., Asbridge, J. R., Bame, S. J., Feldman, W. C., and Hansen, R. T.: 1981, *J. Geophys. Res.* **82**, 5438.
Hundhausen, A. J.: 1993, *J. Geophys. Res.* **98**, 13 177.
Illing, R. M. E. and Hundhausen, A. J.: 1986, *J. Geophys. Res.* **91**, 951.
Korzhov, N. P.: 1977, *Solar Phys.* **55**, 505.
MacQueen, R. M. and Poland, A. I.: 1977, *Solar Phys.* **55**, 143.
Mendoza, B. and Perez-Enriquez, R.: 1993, *J. Geophys. Res.* **98**, 9365.

Poland, A. I.: 1978, *Solar Phys.* **57**, 141.
Sheeley, N. R., Jr. *et al.*: 1997, *Astrophys. J.* **485**, 472.
Svalgaard, L., Wilcox, J. M., and Duvall, T. L.: 1974, *Solar Phys.* **37**, 157.
Thieme, K. M., Marsch, E., Schwenn, R.: 1987, in V. J. Pizzo, T. Holzer, and D. G. Sime (eds.), *Proceedings of the Sixth International Solar Wind Conference*, YMCA of the Rockies Estes Park, pp. 317–321.
Wilcox, John M., and Hundhausen, A. J.: 1983, *J. Geophys. Res.* **88**, 8095.
Wang, Y.-M. *et al.*: 1997, *Astrophys. J.* **485**, 875.
Wang, Y.-M. *et al.*: 1998a, *Astrophys. J.* **498**, L165.
Wang, Y.-M. *et al.*: 1998b, *Astrophys. J.* **508**, 899.
Woo, R., Armstrong, J. W., Bird, M. K., and Patzold, M.: 1995, *Astrophys. J.* **449**, L91.